Data-Driven Reduction
of a Cardiac Myofilament Model

Tommaso Mansi[1], Bogdan Georgescu[1], Jagir Hussan[2], Peter J. Hunter[2],
Ali Kamen[1], and Dorin Comaniciu[1]

[1] Siemens Corporation, Corporate Technology, Imaging and Computer Vision,
Princeton, NJ, USA
[2] Auckland Bioengineering Institute, The University of Auckland, New Zealand

Abstract. This manuscript presents a novel, data-driven approach to
reduce a detailed cellular model of cardiac myofilament (MF) for effi-
cient and accurate cellular simulations towards cell-to-organ computa-
tion. Based on 700 different sarcomere dynamics calculated using Rice
model, we show through manifold learning that sarcomere force (SF) dy-
namics lays surprisingly in a linear manifold despite the non-linear equa-
tions of the MF model. Then, we learn a multivariate adaptive regression
spline (MARS) model to predict SF from the Rice model parameters
and sarcomere length dynamics. Evaluation on 300 testing data showed
a prediction error of less than 0.4 nN/mm^2 in terms of maximum force
amplitude and 0.87 ms in terms of time to force peak, which is com-
parable to the differences observed with experimental data. Moreover,
MARS provided insights on the driving parameters of the model, mainly
MF geometry and cell mechanical passive properties. Thus, our approach
may not only constitute a fast and accurate alternative to the original
Rice model but also provide insights on parameter sensitivity.

1 Introduction

Advances in experimental protocols and in computational modeling of heart
function are enabling the community to investigate functional relationships be-
tween sub-cellular mechanisms and organ function [1,5]. In brief, the output
of detailed sub-cellular models of cardiac myocyte are linked to a multi-scale,
continuum framework [4,11]. Recent numerical schemes, such as the "update"
method [4], can now overcome the numerical instabilities that rise due to the mul-
tiple feedbacks between the models. However, these models are computationally
demanding due to the numerous and coupled algebraic and ordinary differential
equations, which span several temporal and spatial scales (one cell calculation
can take $\approx 1\,s$/heart beat). Another yet important challenge to be addressed
for clinical uses is the personalization of these models to genetic groups, at a
population level (be animal or human), or for a specific patient [5]. To that end,
it is necessary 1) to quantify the sensitivity of model predictions with respect to
their parameters, and 2) to design models whose parameters can be identified,
directly or statistically, from clinical data.

In parallel, model reduction techniques that rely on statistical learning have been investigated, in particular in the chemometrics community. Often referred to as meta-modeling, the idea is to derive a statistical model that is able to capture the output of complex, non-linear computational models while being expressed with fewer parameters and being extremely computationally efficient (computation time in the order of the ms or less) [9]. Meta-modeling has been used to analyze the interactions between parameters [10] but also to estimate them using libraries of models [3]. Partial least squares regression (PLSR) is probably the preferred method owing to its good generalization properties [9]. More advanced manifold learning can also prove useful in that context, as suggested by the excellent performance recently achieved in computer vision [2].

Motivated by the recent model reduction progresses, we aim to develop a data-driven approach to 1) reduce the number of parameters of a multi-scale cellular model of cardiac myofilament (MF) and 2) to learn a data-driven generative model suitable for cell-to-organ simulations while still capturing the output of the original model. To the best of our knowledge, this is the first time such a strategy is applied to multiscale cardiac modeling. In this work, we focus on the sarcomere force (SF) computed by the validated Rice MF model [6] (Sec. 2.1). We first use manifold learning techniques to reduce the dimensionality of SF. Among the tested methods, we report here the results obtained using principal component analysis (PCA) and locally linear embedding (LLE), for which we obtained the best results (Sec. 2.2). Next, we learn a forward, generative model of SF dynamics given a set of Rice model parameters and sarcomere length (SL) dynamics (Sec. 2.3 and Sec. 2.4). As reported in Sec. 3, SF manifold was surprisingly linear despite being the output of a non-linear system: only four PCA components were necessary to capture it. Our generative model also provided promising predictive results while being extremely fast to compute. Furthermore, it suggested a strong effect of MF geometry, cell mechanical passive properties and SL on SF dynamics. Sec. 4 discusses these results and concludes the paper.

2   Methods

2.1   Overview of Cardiac Myofilament Model

The Rice model is a lumped model of cardiac myofilament (MF) especially designed to capture a wide range of experimental observations (see [6] for futher details). In particular, it models the main regulatory processes involved in cross-bridge cycling to compute bulk myoplasmic calcium transient ($[Ca^{2+}]$), sarcomere length (SL), sarcomere force (SF) and their inter-dependence over the cardiac cycle.

From a dynamic system point of view (Fig. 1, left panel), the input $\mathbf{u}(t)$ at time t of the system comprises $n_p = 39$ free constant parameters $\theta \in \mathbb{R}^{n_p}$, the large majority being related to sub-cellular mechanisms, and a time varying trans-membrane potential $v(t)$, which can be computed using any cellular electrophysiology model [8]. System states $\mathbf{x}(t)$ are $SL(t)$, shortening velocity $SV(t)$, $[Ca^{2+}](t)$, and the numerous transition rates $\kappa_i(t)$ that characterize the
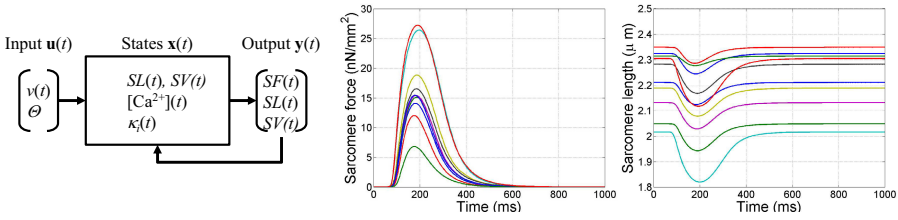
Fig. 1. *Left panel*: Dynamic system schematic of the Rice model (see text for details). *Mid and Right panels*: ten examples of sarcomere force (SF) and sarcomere length (SL) simulations over one heart cycle.

cross-bridge cycle. The output $\mathbf{y}(t)$ is $SL(t)$, $SV(t)$ and $SF(t)$. Importantly, the system presents with a feedback loop as SF results in SL and SV changes (see Eq. 38 in [6]). The model comprises 64 coupled ODE's, which makes its resolution at the organ scale particularly challenging. In this study, the potential $v(t)$ is fixed as we are interested in MF dynamics only. As a result, all simulations are temporally registered by construction. Furthermore, we focus on the steady SF dynamics: analysis of transient phenomena are subject of future work.

2.2 Sarcomere Force Manifold Analysis through Model Reduction

First, we analyze the dimensionality of the SF manifold Ω_{SF}, i.e. the number of intrinsic parameters $n_q \neq n_p$ that are necessary to capture the observed $SF(t)$ (the reader is referred to [2] for details on statistical learning and the methods used in the following sections). Let N be the number of simulations (the observations). For each observation i, $SF^i(t)$ is calculated with a unique set of parameters θ^i and sampled in n_s samples ($t \in [t_0, t_{end} = n_s dt]$, where t_0, t_{end} and dt are the initial time, final time and time step of the observed cardiac cycle respectively). We define the observation vector $\mathbf{y}^i = [SF^i(t_0) \dots SF^i(t_{end})] \in \mathbb{R}^{n_s}$, which are gathered in an $N \times n_s$ observation matrix Y. To identify potential nonlinear structures, several manifold learning techniques were tested. We report here the two methods that provided best results in terms of data compression while being interpretable.

Principal Component Analysis. (PCA) computes the reduced space Ω_{SF}^{pca} by finding the orthonormal basis formed by the principal components $\mathbf{v}_l^T, l \in \{1 \dots n_s\}$, that maximizes the observed covariance [2]. The $\mathbf{v}_l^T$'s are the eigenvectors of the covariance matrix $(Y - \bar{\mathbf{y}})(Y - \bar{\mathbf{y}})^T$, ordered by decreasing energy ($\bar{\mathbf{y}} = 1/N \sum_{i=1}^N \mathbf{y}^i$). Dimensionality reduction is achieved by choosing a reduced set of components $\mathbf{v}_l^T, l \in \{1 \dots n_q\}, n_q \leq n_p \ll n_s$ and by projecting the observations onto that new space, $\mathbf{z}_{pca}^i = (\mathbf{y}^i - \bar{\mathbf{y}})V$, where V is the matrix $V = (\mathbf{v}_1^T \dots \mathbf{v}_{n_q}^T)$. Now, given new PCA coefficients $\hat{\mathbf{z}}_{pca}$, the related $\hat{SF}(t)$ encoded by the vector $\hat{\mathbf{y}} \in \Omega_{SF}$ is reconstructed through $\hat{\mathbf{y}} = \bar{\mathbf{y}} + \hat{\mathbf{z}}_{pca}V$.

Locally Linear Embedding. (LLE) [7] calculates a low-dimensional space Ω_{SF}^{lle} that preserves the barycentric coordinates of each data point with respect

to its k_{lle} nearest neighbors. Because the mapping is computed using local neighborhoods, the method can capture non-linear manifold structures. The algorithm has three steps: 1) find the k_{lle} nearest neighbors of each data point $\mathbf{y}^i$, $\{\mathbf{y}^{\mathcal{N}^{k_{lle}}(\mathbf{y}^i)}\}$, according to the Euclidean distance; 2) compute the barycentric coordinates $\mathbf{w}^i$ of $\mathbf{y}^i$ with respect to the k_{lle} neighbors; 3) compute the embedding coordinates $\mathbf{z}_{lle}^i \in \Omega_{SF}^{lle}$ of $n_q \leq n_p \ll n_s$ dimensions using the barycentric coordinates $\mathbf{w}^i$, which amounts to solving an eigenvalue problem. Although LLE does not provide an explicit mapping between Ω_{SF} and Ω_{SF}^{lle}, it can be extended to new data easily by taking advantage of the preservation of the barycentric coordinates. Let $\hat{\mathbf{y}}$ be a new data sample in Ω_{SF}. We first find its k_{lle} nearest neighbors within the training set. The barycentric coordinates $\hat{\mathbf{w}}$ are calculated and used as interpolation weights to estimate the embedding coordinates $\hat{\mathbf{z}}_{lle} \in \Omega_{SF}^{lle}$ from those of the k_{lle} nearest neighbors. New observations $\hat{\mathbf{y}}$ are reconstructed from the embedding coordinates $\hat{\mathbf{z}}_{lle}$ in a similar way.

2.3   Static, Data-Driven Model of Sarcomere Force

We then learn a data-driven model of SF from the computed simulations. As in Sec. 2.2, the dynamics of the problem is ignored at this stage: all variables are known throughout the cardiac cycle. Sec. 2.4 extends the method to predict $SF(t_c + dt)$ given θ and $SL(t), t \in [t_0, t_c]$.

Model Input. In addition to the free parameters θ, we also consider $SL(t)$ as an input of our model to capture SL dependence on SF. This assumption is not limiting as SL is an observable state of the MF system (Fig. 1). Because consecutive SL values over time are highly correlated, we express SL in terms of PCA coefficients $\mathbf{z}_{SL} \in \Omega_{SL}^{pca} = \mathbb{R}^{n_{SL}}$, with $n_{SL} \ll n_s$.

Model Output. To optimize model construction, the reduced SF representation computed in Sec. 2.2 is considered as output: Our model predicts the embedding coordinates $\mathbf{z}$, which are then used to reconstruct the SF curve $\mathbf{y}$.

Model Estimation. Based on the previous assumptions, the data-driven model to estimate writes $\mathbf{z} = \mathbf{f}(\theta, \mathbf{z}_{SL})$, $\mathbf{f} : \mathbb{R}^{n_p} \times \mathbb{R}^{n_{SL}} \mapsto \mathbb{R}^{n_q}$. In this study, $\mathbf{f}$ is estimated using multivariate adaptive regression splines (MARS), a non-parametric regression methods with explicative capabilities [2]. Intuitively, MARS extends linear regression by fitting splines (linear or cubic) to the predictors to capture data non-linearities and variable interactions. The model is estimated in two steps. A forward pass fits the splines to the data in a greedy approach such that the mean square error (MSE) on the training set diminishes. The backward pass, which aims to minimize over-fitting and optimize generality, prunes the model by removing the splines that less decrease MSE. This step, similar to model selection techniques in linear regression, enables one to identify the most relevant predictors in the model, thus providing indications on the input parameters that have most impact on SF dynamics. In this work, $\mathbf{f}$ is estimated component-wise, i.e. $\mathbf{f} = [f_1 \ldots f_{n_q}]$, the $f_{k \in \{1 \ldots n_q\}} : \mathbb{R}^{n_p} \times \mathbb{R}^{n_{SL}} \mapsto \mathbb{R}$ being n_q independent MARS models. The most important parameters of the MARS algorithm to setup are

the maximum number of splines included in the model ($maxFun$), the penalty weight (c) and the number of variable interactions ($vInt$).

Prediction Algorithm. The final prediction algorithm is as follows. We first project $\hat{SL}(t)$ onto Ω_{SL}^{pca}, yielding the reduced representation $\hat{\mathbf{z}}_{SL}$. We then compute $\hat{\mathbf{z}} = \mathbf{f}(\hat{\theta}, \hat{\mathbf{z}}_{SL})$ and reconstruct SF from $\hat{\mathbf{z}}$ as described in Sec. 2.2.

2.4   Extension to the Dynamic Scenario

In practice, sarcomere length $SL(t)$ is known from $t = [t_0, t_c]$ only (t_c is the current time). We thus adapt the previous framework to the dynamic scenario as follows. Intuitively, we use the past SL dynamics to find the closest training candidates on the SF manifold. We then use these candidates to predict the entire SL dynamics, which is finally utilized as input to our forward model to compute SF at the next time steps. Let $\mathbf{x}_{SL}$ be the vector of dimension $n_{t_c} < n_s$ that encodes $SL(t), t \in [t_0, t_c]$. We first find the k closest SL dynamics $\mathbf{x}_{SL_{train}}^{\mathcal{N}(\mathbf{x}_{SL})}$ within the training set from $\mathbf{x}_{SL}$ based on the Euclidean distance computed between t_0 and t_c, denoted $d^{\mathcal{N}(\mathbf{x}_{SL})}$. To ensure smooth predictions, we compute the interpolated SL, $\mathbf{x}_{SL_{train}} = \sum_j \left(d_j^{\mathcal{N}(\mathbf{x}_{SL})} \right)^{-2} \mathbf{x}_{SL_{train},j}^{\mathcal{N}(\mathbf{x}_{SL})}$. We then replace the values of $\mathbf{x}_{SL_{train}}$ between $t = [t_0, t_c]$ by those of the actual $\mathbf{x}_{SL}$ and project the result into the SL subspace Ω_{SL}^{pca} to get the predicted coordinates $\mathbf{z}_{SL}$. We finally compute $\mathbf{z} = \mathbf{f}(\theta, \mathbf{z}_{SL})$ and reconstruct SF from $\mathbf{z}$ to determine $SF(t_c + dt)$, which can then be used to calculate $SL(t_c + dt)$ (according to the constitutive law of the whole-heart model for instance). The process is iterated throughout time-steps to compute the entire SF dynamics.

3   Experiments and Results

The Rice MF model was computed using the freely available source code provided by the authors[1]. The setup used to get Fig. 9 in [6] was employed except that trabeculae dynamics was computed instead of single cell to be as close as possible to the whole-heart scenario. MF cross-bridge was coupled to the Chicago model of cardiac electrophysiology [8] and computed at 37° C. 1000 MF simulations were calculated by randomly varying the 39 MF parameters between $\pm 10\%$ of their original values according to a uniform distribution (see Table 1 in [6]), with the following constraints to ensure physiologically plausible simulations:

- The length of the thin filament was $length_{thin} = SL_{max}/2$
- The length of the thick filament $length_{thick}$ was always shorter than SL_{max}
- SL at rest was midway between SL_{max} and SL_{min}
- Initial SL was $SL_{set} = SL_{min} + 0.8\,(SL_{max} - SL_{min})$, as in [6]
- Collagen effects started at $SL_{col} = SL_{min} + 0.85\,(SL_{max} - SL_{min})$, as in [6].


Non-reported experiments with fewer simulations yielded similar results. Ten cycles were computed at 1 beat/s to reach steady state but only the last cycle was considered for the statistical analyses. Numerical noise in SF was smoothed out using Fourier transform by zeroing the 101th and beyond Fourier coefficients. Finally, the dataset was randomly split into training (70% of the observations) and testing sets for unbiased evaluation. Two metrics were employed to estimate the goodness of fit of the predicted SF: Maximum Amplitude Difference (MAD, in nN/mm^2) and Time to Peak Difference (TPD, in ms), defined by $MAD(\mathbf{y}^i, \mathbf{y}^j) = |\max(\mathbf{y}^i(t)) - \max(\mathbf{y}^j(t))|$ and $TPD(\mathbf{y}^i, \mathbf{y}^j) = |\operatorname{argmax}_t(\mathbf{y}^i(t)) - \operatorname{argmax}_t(\mathbf{y}^j(t))|$. In the following, values are reported as mean $\pm$ SD (90-tile). MAD and TPD variations around the mean were 5.64 ± 3.89 (11.29) nN/mm^2 and 5.9 ± 4.32 (11) ms respectively. Fig. 1, mid and right panels illustrate some examples of SF and SL dynamics.
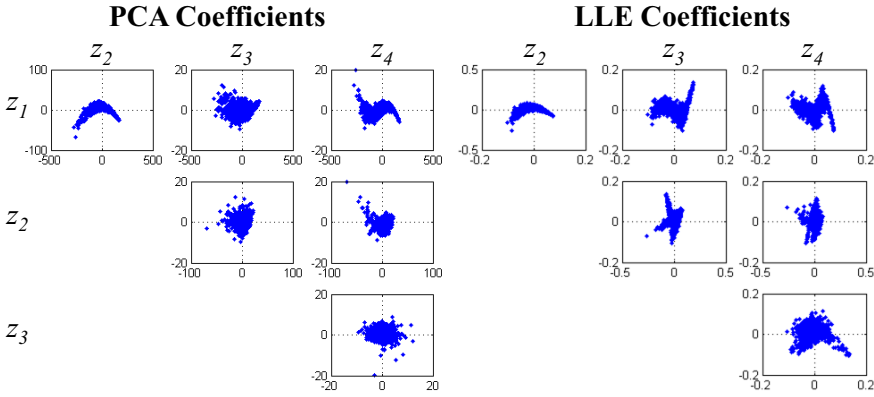
Fig. 2. Pairwise plot of data coefficients in the estimated subspaces. PCA and LLE distributions are qualitatively similar, suggesting a linear SF manifold.

Sarcomere Force Manifold Analysis. PCA and LLE spaces were computed using the training set. Four PCA components were sufficient to capture SF dynamics. Successive projection / reconstruction of the testing set yielded an MAD of 0.92 ± 0.83 (1.84) % of MAD standard deviation between reconstructed and ground truth and a TPD of 0.81 ± 0.84 (2) ms was obtained. Thus, both peak value and time to peak could be accurately captured by PCA reduction. LLE reached the same accuracy with four components as well when the number k_{lle} of neighbors became higher than 20 (results were worse for $k_{lle} < 20$ and $n_q < 4$). With $k_{lle} = 20$, testing accuracy was 1.23 ± 1.32 (2.76) % for MAD and 1.12 ± 1.22 (2) ms for TPD. This result, along with pair-wise plots of embedding coefficients (Fig. 2) surprisingly suggested a linear structure of the SF manifold, although SF was the result of a non-linear model. Indeed, both LLE and PCA coefficients exhibited similar distribution patterns (Fig. 2). As a result, using non-linear manifold learning did not bring much information. We could draw similar
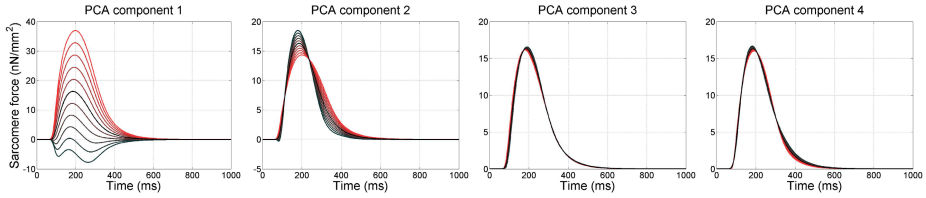
Fig. 3. Modes of variation around the mean of the first four PCA components, from -3 SD (black) to $+3$ SD (red). See text for detail.

conclusions using other manifold learning techniques like ISOMAP (non reported here). Fig. 3 illustrates the modes of SF variations estimated by PCA. In particular, the first mode captured SF amplitude, whereas the second one captured variations in time to peak due to different contraction and relaxation patterns. It should be noted that the non-physiologial SF behavior captured by the first mode at large negative coefficients can be easily avoided by using explicit thresholding. Based on these results, we used PCA model reduction in all subsequent experiments.

Evaluation of the Data-Driven Forward Model. We then estimated the forward model $\mathbf{z}_{pca} = \mathbf{f}(\theta, \mathbf{z}_{SL})$ from the training set. Five PCA coefficients were enough to capture SL, $n_{SL} = 5$. Using 5-fold cross-validation on the training set, we identified the optimal MARS parameters: $c = 2$, $vInt = 2$ and $maxFun = 50, 80, 80$ and 70 for the first, second, third and fourth PCA component respectively. We also estimated two additional models: $\mathbf{f}_\theta$ whose input was θ only, and $\mathbf{f}_{SL}$ whose input was SL only. We then evaluated the predictive power of each model on the testing set. As one can see from Table 1, both SL and θ were necessary to correctly estimate SF dynamics. This result agrees with the feedback process of the MF model. Quantitatively, obtained predictions were very promising, both in terms of maximum amplitude (absolute average MAD of 0.15 nN/mm^2) and time to peak (average TPD of 0.87ms), comparable to differences reported with experimental data. The good performances of the model could also be verified qualitatively, as illustrated in Fig. 4. Interestingly, ANOVA analysis on the MARS model [2] showed that the driving input parameters were mostly related to sarcomere geometry, SL dynamics, passive properties, and at a lower extents to cross-bridge detachment. This finding may guide further model reduction strategies.

We finally tested the proposed dynamic model. In this first experiment, we used the precomputed SL, i.e. we did no update $SL(t + dt)$ according to the predicted $SF(t + dt)$ (this step is subject of future work). In that way, we could quantify the predictive power of the model in terms of SF exclusively, without being influenced by potentially changing SL dynamics. As it can be seen from Table 1, the proposed dynamic algorithm achieved promising predictions, with absolute average MAD of 0.35 nN/mm^2. These results are encouraging towards full integration of our data-driven model into rheological continuous frameworks.
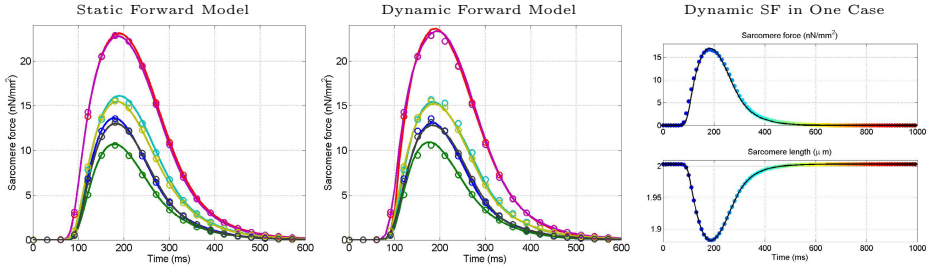
Fig. 4. Data-driven SF results on seven randomly selected testing data (*left and middle panels*) and one typical case (*right panel*) (input: θ and SL). As one can see, the model was able to compute SF accurately *(plain line: prediction, circles: ground truth)*. Right panel shows computed SF dynamics (colors encode time, ground truth in black).

Table 1. Performances of data-driven forward models. Both SL and θ, the free parameters, are necessary to predict SF accurately (MAD in % of data SD). Good performances are still achieved even in the dynamic scenario.

	90-ptile	Median	Mean	SD	90-ptile	Median	Mean	SD
	Input: θ (static)				**Input: θ and SL (static)**			
MAD (%)	20.52	7.31	9.52	8.20	8.43	2.83	3.91	4.30
TPD (ms)	3	1	2	8.77	2	1	0.87	1.58
	Input: SL (static)				**Input: θ and SL (dynamic)**			
MAD (%)	46.41	15.06	20.74	19.35	16.75	6.37	8.35	8.44
TPD (ms)	2	1	1.05	3.79	1	0	0.32	0.55

4 Discussion and Conclusion

In this paper, we have proposed a manifold learning method to identify the intrinsic dimensionality of the SF manifold computed by the Rice model and learn, for the first time to the best of our knowledge, a forward model of SF. Our first, surprising finding is that SF appears to lay on a linear manifold despite being generated by complex non-linear systems. Moreover, two of the identified PCA components have a clear dynamic signature, which could be used to infer MF parameters from observations. The second important finding is that data-driven approaches are able to capture the dynamics of complex cellular models, here SF. By learning the observed dynamics, we could reproduce it without having to explicitly solve the complex ODEs involved in cellular models. Various methods have been tried, like partial least squares or gradient boosting trees. The MARS method yielded the most promising prediction accuracy, while being computationally efficient (the evaluation of one cycle takes milliseconds in Matlab). It also suggested that the main parameters that drive SF are related to the geometry of the sarcomere, SL dynamics, passive properties and cross-bridge detachment. In this study, we chose to vary all parameters around $\pm 10\%$ of their nominal value as a first step. In the future, parameters would need to be studied on a case by case basis based on the observed variations in experimental setups.

For such studies, the method discussed in this paper allows for creation of a series of reduced models that could be invoked in the appropriate ranges. Finally, shortening velocity (SV) was implicitly taken into account through SL curves. Explicit modeling of SV may improve prediction accuracy, which we will investigate in future work. In conclusion, our approach can provide efficient reduced models while still being accurate, opening the way to efficient cell-to-whole-heart frameworks for -omics / phenotype studies.

References

1. Campbell, S., McCulloch, A.: Multi-scale computational models of familial hypertrophic cardiomyopathy: genotype to phenotype. Journal of The Royal Society Interface 8(64), 1550–1561 (2011)
2. Friedman, J., Hastie, T., Tibshirani, R.: The Elements of Statistical Learning: Data Mining, Inference, and Prediction. Springer, New York (2009)
3. Isaeva, J., Sæbo, S., Wyller, J., Nhek, S., Martens, H.: Fast and comprehensive fitting of complex mathematical models to massive amounts of empirical data. Chemometrics and Intelligent Laboratory Systems (2011)
4. Land, S., Niederer, S., Smith, N.: Efficient computational methods for strongly coupled cardiac electromechanics. IEEE TBE 59(5), 1219–1228 (2012)
5. Niederer, S., Land, S., Omholt, S., Smith, N.: Interpreting genetic effects through models of cardiac electromechanics. American Journal of Physiology-Heart and Circulatory Physiology 303(11), H1294–H1303 (2012)
6. Rice, J., Wang, F., Bers, D., De Tombe, P.: Approximate model of cooperative activation and crossbridge cycling in cardiac muscle using ordinary differential equations. Biophysical Journal 95(5), 2368–2390 (2008)
7. Roweis, S., Saul, L.: Nonlinear dimensionality reduction by locally linear embedding. Science 290(5500), 2323–2326 (2000)
8. Shannon, T., Wang, F., Puglisi, J., Weber, C., Bers, D.: A mathematical treatment of integrated ca dynamics within the ventricular myocyte. Biophysical journal 87(5), 3351–3371 (2004)
9. Tøndel, K., Indahl, U., Gjuvsland, A., Vik, J., Hunter, P., Omholt, S., Martens, H.: Hierarchical cluster-based partial least squares regression (HC-PLSR) is an efficient tool for metamodelling of nonlinear dynamic models. BMC Systems Biology 5(1), 90 (2011)
10. Tøndel, K., Vik, J., Martens, H., Indahl, U., Smith, N., Omholt, S.: Hierarchical multivariate regression-based sensitivity analysis reveals complex parameter interaction patterns in dynamic models. Chemometr. Intell. Lab (2012)
11. Williams, G., Smith, G., Sobie, E., Jafri, M.: Models of cardiac excitation–contraction coupling in ventricular myocytes. Math. Biosci. 226(1), 1–15 (2010)